Journal of Hydrology 446–447 (2012) 48–58

Contents lists available at SciVerse ScienceDirect

Journal of Hydrology

journal homepage: www.elsevier.com/locate/jhydrol

An analytical solution for a radial collector well near a stream with a low-permeability streambed

Ching-Sheng Huang, Pei-Rong Tsou, Hund-Der Yeh *

Institute of Environmental Engineering, National Chiao Tung University, Hsinchu, Taiwan

ARTICLE INFO

Article history:
Received 13 July 2011
Received in revised form 9 April 2012
Accepted 14 April 2012
Available online 2 May 2012
This manuscript was handled by Phillipe Baveye, Editor-in-Chief, with the assistance of Xunhong Chen, Associate Editor

Keywords:
General trigonometrical kernel
Laplace transform
Stream depletion rate
Third-type boundary

SUMMARY

Radial collector wells are often constructed near a stream to obtain more water and produce smaller drawdown in comparison with traditional vertical wells. This paper aims at developing a mathematical model for describing head distributions induced by pumping in a radial collector well near a stream in an unconfined aquifer. A low permeable streambed between the stream and the aquifer is considered. The first-order free surface equation is used to describe the movement of water table. A point-sink solution of the model is developed first by a general transform combining Fourier sine and cosine transforms and then by Fourier transform and Laplace transform. The transient solution of head distributions for different well types such as the horizontal well or radial collector well can be obtained by integrating the point-sink solution along the well. Based on Darcy's law and the developed solution, an equation for temporal stream depletion rate describing filtration from the stream is then obtained. The steady-state solutions for filtration can be obtained from the transient solution when neglecting the exponential term associated with time. It is found that steady-state filtration depends only on the ratio of streambed permeability over aquifer permeability. Steady-state filtration equals water extraction from a well when the ratio is larger than 10^{-2}. The streambed is regarded as completely impermeable when the ratio is less than 10^{-7}. Additionally, the lowest water table happens near the well before occurrence of filtration. The lowest water table moves landward and away from the well after filtration occurs.

1. Introduction

Radial collector wells have been commonly designed and used to collect water from a nearby stream. The radial collector well designed by Ranney Leo was developed from horizontal wells in 1930s (Hunt, 2006). A radial collector well generally comprises a central reinforced concrete caisson and several laterals under the ground surface. The central caisson is drilled downward with an inside diameter ranging from 3 to 6 m or larger, and the laterals horizontally extend from the central caisson at a proper depth in an aquifer. The groundwater flows through the laterals to the caisson if the radial collector well starts pumping.

Some researchers built a model or executed an experiment to simulate groundwater flow due to pumping in a collector well. Mikels and Klaer (1956) mentioned that a radial collector well can be approximated as one vertical well with a radius of 75–80% of its lateral length. McWhorter and Sunada (1977) also mentioned that one vertical well with a radius of 61% of lateral length could approximate a radial collector well. Bischoff (1981) used a boundary element method to simulate groundwater movement due to pumping in a radial collector well with three laterals in a confined aquifer near a stream. Bakker et al. (2005) presented a multilayer analytic element method for approximating groundwater flow to radial collector wells. They indicated that groundwater flow can be simulated accurately by using such a method. Patel et al. (2010) used an analytic element method to simulate steady-state discharge due to a radial collector well in an unconfined aquifer. The pumping rate along the lateral is considered to vary in space rather than keep a constant. Based on this method, they provided an empirical equation to describe discharge from a radial collector well. Dugat (2009) constructed a numerical model to investigate groundwater flow to a radial collector well near a stream in an unconfined aquifer. He indicated that the pumping rate is an important factor to determine the quantity of pumped water from background aquifer. Su et al. (2007) used a numerical model to simulate an unsaturated region occurring between the bottom of a partially-penetrating stream and the water table due to pumping in two radial collector wells beneath the stream. They found that the unsaturated region increases with the ratio of hydraulic conductivity of the aquifer to that of streambed. Kim et al. (2008) carried out sand-tank experiments of a collector well consisting of one caisson and one lateral. Their results showed that the water pumped from the caisson increases if the lateral length

* Corresponding author. Address: 300 Institute of Environmental Engineering, National Chiao Tung University, 1001 University Road, Hsinchu, Taiwan. Fax: +886 35 726050.
E-mail address: hdyeh@mail.nctu.edu.tw (H.-D. Yeh).

0022-1694/$ - see front matter © 2012 Elsevier B.V. All rights reserved.
http://dx.doi.org/10.1016/j.jhydrol.2012.04.028

or diameter increases or if the water level in the caisson decreases. Mohamed and Rushton (2006) developed a two dimensional (2D) numerical model to calculate groundwater head due to a single horizontal well. In their model, the effects of well diameter and screen permeability were considered, and Hazen–Williams expression was employed to account for the flow within the well. In addition, they also carried out a field experiment to confirm their model.

Some semi-analytical and analytical solutions had been proposed to describe the groundwater flow and stream depletion rate (SDR) to collector wells. The SDR is defined as the ratio of filtration from a stream to water extraction from a pumping well. The SDR is zero initially before a drawdown cone touches a stream and then increases gradually with time. Finally, the SDR approaches one, indicating that the SDR reaches steady state and filtration from a stream is equal to water extraction from a well. Hantush and Papadopoulos (1962) presented analytical solutions in terms of well function to describe drawdown distribution due to pumping in a radial collector well in an unconfined aquifer. The aquifer is homogeneous, isotropic and of infinite extent in the horizontal direction. Their drawdown solution for the presence of a stream is obtained by the use of the method of images and therefore not capable of considering a streambed effect on SDR or hydraulic head. They reported that more laterals of the collector well result in smaller drawdown. Javandel and Zaghi (1975) developed a semi-analytical solution for describing head distributions induced from a fully-penetrating well of a finite radius in a confined aquifer. The bottom of the well has a finite-thickness disk with a larger radius than the well. Sun and Zhan (2006) proposed a semi-analytical solution to describe water filtration from a reservoir to a single horizontal well. The well was installed under the reservoir and extended infinitely in the horizontal direction. A finite-thickness aquitard between the aquifer and reservoir was considered to have vertical flow and specific storage. Tsou et al. (2010) derived analytical solutions to investigate head distributions and SDR induced from pumping in a slanted well in a confined aquifer near a fully-penetrating stream. Similarly, Huang et al. (2011) developed analytical solutions for head distributions and SDR in unconfined aquifer cases and investigated the behaviors of the SDR. However, both articles neglect the effect of a low permeable streambed in the development of the solutions for the hydraulic head and SDR.

The objective of this paper is to develop a mathematical model for describing head distributions due to pumping in a radial collector well near a fully-penetrating stream in an unconfined aquifer. A low permeable streambed is considered along the edge of the stream; the stream is, therefore, treated as a third-type boundary condition in the model. A first-order free surface equation is employed to describe the vertical movement of the phreatic surface. The head solution of the model is obtained by applying Fourier transform, Laplace transform and $\Re$-transform which includes the kernel functions of Fourier sine and cosine transforms. The SDR is then derived based on the head solution and Darcy's law. The head distributions due to pumping in a radial collector well predicted by the present solution are compared with those of Hantush and Papadopulos' solution (1962) and Hantush's solution (1965). In addition, the water levels predicted by the present solution are compared with observed field data of Schafer (2006) and Jasperse (2009) to demonstrate the applicability of the present solution to real-world problems. With the aid of the present solution, the effects of the configuration of laterals on the SDR and head distributions at phreatic surface are investigated. Moreover, the effects of the streambed permeability on the SDR and water table distributions are also examined.

2. Methodology

2.1. Conceptual model

Fig. 1 shows the schematic representation for a three dimensional (3D) conceptual model of a radial collector well in an anisotropic unconfined aquifer near a stream. According to Jacob (1950) as well as Todd and Mays (2005), a shallow stream or a partially-penetrating stream can approximate a fully-penetrating one if the distance between a stream and well is greater than 1.5 times aquifer thickness. A fully-penetrating stream is therefore considered in the conceptual model. A semi-pervious material along the stream edge is treated as the streambed which connects the stream and aquifer. The origin of the coordinate system is located at the interface between the aquifer and streambed. The top of the stream is considered as a reference datum. The collector well consists of a central vertical caisson with a large diameter and several horizontal lateral pipes, each of which may have different length L. The θ represents an angle between the positive x-direction and the lateral adjacent to the horizontal axis. The distance between the center of the collector well and the stream edge is x_0, and the depth measured form the stream surface to horizontal laterals is z_0. The aquifer is of a depth H, and the thickness of the streambed is b'.

Three assumptions made in the model are as follows: 1. The aquifer is homogenous. 2. The discharge intensity is assumed to be uniformly distributed along all of laterals. 3. The stream stage does not change during the pumping period, indicating that the stream water is much more than the pumped water. For the problem with a variable stream, readers can refer to Intaraprasong and Zhan (2009).

The point-sink solution for the model described above is developed herein. The governing equation describing 3D transient hydraulic head distributions with a point sink can be expressed

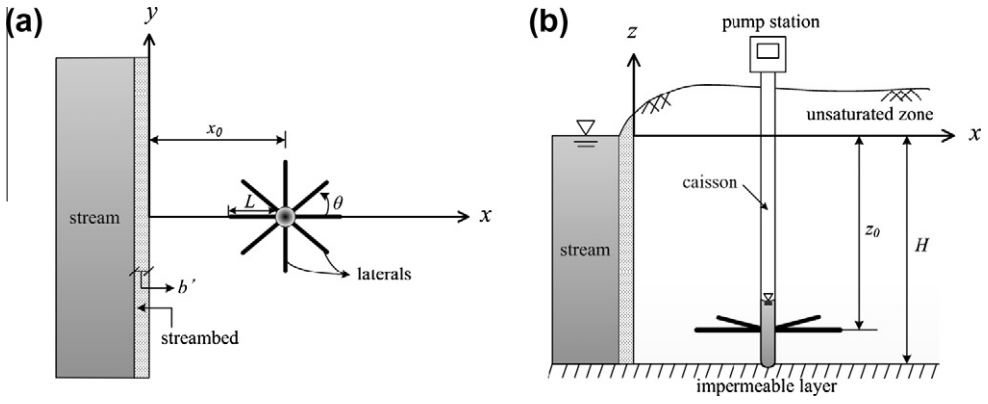

Fig. 1. Schematic diagram of a radial collector well in an unconfined aquifer near a stream with a streambed (a) top view (b) cross section view.

as (Tsou et al., 2010)

$$K_x\frac{\partial^2 h}{\partial x^2}+K_y\frac{\partial^2 h}{\partial y^2}+K_z\frac{\partial^2 h}{\partial z^2}=S_s\frac{\partial h}{\partial t}+Q\delta(x-x')\delta(y-y')\delta(z-z') \quad (1)$$

where K_x, K_y and K_z are hydraulic conductivities in x-, y- and z-direction, respectively; S_s is specific storage; Q is a positive constant pumping rate; $\delta()$ represents Dirac delta function and (x', y', z') is the coordinate of the point sink.

The permeability K' of the streambed may be equal to or lower than that of the aquifer. The edge of the streambed is therefore considered as a third-type boundary condition for the model and expressed as

$$K_x\frac{\partial h}{\partial x}-\frac{K'}{b'}h=0 \quad at \quad x=0 \quad (2)$$

Note that Eq. (2) reduces to a constant-head condition if the thickness of streambed equals zero. The remote boundary conditions in x- and y-direction are, respectively, denoted as

$$\lim_{x\to\infty} h=0 \quad (3)$$

and

$$\lim_{y\to\pm\infty} h=0 \quad (4)$$

The bottom of the unconfined aquifer is under a no-flow condition and thus expressed as

$$\frac{\partial h}{\partial z}=0 \quad at \quad z=-H \quad (5)$$

The top boundary describing the movement of the water table without surface recharge is approximately expressed as (Yeh et al., 2010)

$$S_y\frac{\partial h}{\partial t}=-K_z\frac{\partial h}{\partial z} \quad at \quad z=0 \quad (6)$$

which neglects second-order terms since the stream provides a part of pumped water and the change of the water table may not be large.

The initial condition is expressed as

$$h=0 \quad \text{at} \quad t=0 \quad (7)$$

which indicates no groundwater flow before pumping.

The dimensionless variables are introduced as follows:

$$\begin{aligned} &x_D=\frac{x}{H}, \quad y_D=\frac{y}{H}, \quad z_D=\frac{z}{H}, \quad x'_D=\frac{x'}{H}, \quad y'_D=\frac{y'}{H}, \quad z'_D=\frac{z'}{H}\\ &x_{0D}=\frac{x_0}{H}, \quad y_{0D}=\frac{y_0}{H}, \quad z_{0D}=\frac{z_0}{H}, \quad L_D=\frac{L}{H}\\ &t_D=\frac{K_x}{H^2S_s}t, \quad h_D=\frac{\pi^2K_xH}{Q}h \end{aligned} \quad (8)$$

According to Eq. (8), the governing Eq. (1) leads to

$$\frac{\partial^2 h_D}{\partial x_D^2}+\kappa_y\frac{\partial^2 h_D}{\partial y_D^2}+\kappa_z\frac{\partial^2 h_D}{\partial z_D^2}=\frac{\partial h_D}{\partial t_D}+\pi^2\delta(x_D-x'_D)\delta(y_D-y'_D)\delta(z_D-z'_D) \quad (9)$$

where $\kappa_y = K_y/K_x$ and $\kappa_z = K_z/K_x$.

Similarly, the boundary conditions and initial condition can be rewritten as

$$\frac{\partial h_D}{\partial x_D}+\alpha h_D=0 \quad \text{at} \quad x_D=0 \quad (10)$$

$$\lim_{x\to\infty} h_D=0 \quad (11)$$

$$\lim_{y\to\pm\infty} h_D=0 \quad (12)$$

$$\frac{\partial h_D}{\partial z_D}=0 \quad \text{at} \quad z_D=-1 \quad (13)$$

$$\gamma\frac{\partial h_D}{\partial t_D}=-\kappa_z\frac{\partial h_D}{\partial z_D} \quad \text{at} \quad z_D=0 \quad (14)$$

$$h_D=0 \quad \text{at} \quad t_D=0 \quad (15)$$

where $\alpha = -K'H/(K_xb')$ and $\gamma = S_y/(S_sH)$.

2.2. Head distribution solutions

Applying $\Re$-transform, Fourier transform and Laplace transform to Eqs. (9)–(15) and inverting the result yield the point-sink solution shown below. For the detailed derivation, readers can refer to Appendix A.

$$\begin{aligned} h_{Da}(x_D,y_D,z_D,t_D)=2\int_0^\infty\int_0^\infty &(\Phi_s(z_D)+\Phi_0(z_D,t_D)\\ &+\sum_{n=1}^{\infty}\Phi_n(z_D,t_D))R(x_D)F(y_D)d\xi d\omega\\ &\text{for} \quad z'_D\leqslant z_D\leqslant 0 \end{aligned} \quad (16)$$

$$\begin{aligned} h_{Db}(x_D,y_D,z_D,t_D)=2\int_0^\infty\int_0^\infty &(\Psi_s(z_D)+\Psi_0(z_D,t_D)\\ &+\sum_{n=1}^{\infty}\Psi_n(z_D,t_D))R(x_D)F(y_D)d\xi d\omega\\ &\text{for} \quad -1\leqslant z_D\leqslant z'_D \end{aligned} \quad (17)$$

with

$$\Phi_s(z_D)=-\frac{\cosh(z_D\lambda_s)\cosh[(1+z'_D)\lambda_s]}{\kappa_z\lambda_s\sinh(\lambda_s)} \quad (18)$$

$$\Phi_0(z_D,t_D)=\frac{2\cosh[(1+z'_D)\beta_0](-\beta_0\kappa_z\cosh(z_D\beta_0)+\gamma\lambda_0\sinh(z_D\beta_0)}{\lambda_0[(1+2\gamma)\beta_0\kappa_z\cosh(\beta_0)+(\kappa_z+\gamma\lambda_0)\sinh(\beta_0)]}e^{\lambda_0 t_D} \quad (19)$$

$$\Phi_n(z_D,t_D)=\frac{2\cos[(1+z'_D)\beta_n](\beta_n\kappa_z\cos(z_D\beta_n)+\gamma\lambda_n\sin(z_D\beta_n)}{\lambda_n[(1+2\gamma)\beta_n\kappa_z\cos(\beta_n)-(\kappa_z+\gamma\lambda_n)\sin(\beta_n)]}e^{-\lambda_n t_D} \quad (20)$$

$$\Psi_s(z_D)=-\frac{\cosh(z'_D\lambda_s)\cosh[(1+z_D)\lambda_s]}{\kappa_z\lambda_s\sinh(\lambda_s)} \quad (21)$$

$$\Psi_0(z_D,t_D)=\frac{2\cosh[(1+z_D)\beta_0](-\beta_0\kappa_z\cosh(z'_D\beta_0)+\gamma\lambda_0\sinh(z'_D\beta_0)}{\lambda_0[(1+2\gamma)\beta_0\kappa_z\cosh(\beta_0)+(\kappa_z+\gamma\lambda_0)\sinh(\beta_0)]}e^{\lambda_0 t_D} \quad (22)$$

$$\Psi_n(z_D,t_D)=\frac{2\cos[(1+z_D)\beta_n](\beta_n\kappa_z\cos(z'_D\beta_n)+\gamma\lambda_n\sin(z'_D\beta_n)}{\lambda_n[(1+2\gamma)\beta_n\kappa_z\cos(\beta_n)-(\kappa_z+\gamma\lambda_n)\sin(\beta_n)]}e^{-\lambda_n t_D} \quad (23)$$

$$R(x_D)=\frac{\alpha^2\sin(\omega x'_D)\sin(\omega x_D)-\alpha\omega\sin[(x_D+x'_D)\omega]+\omega^2\cos(\omega x'_D)\cos(\omega x_D)}{\alpha^2+\omega^2} \quad (24)$$

$$F(y_D)=\cos[(y_D-y'_D)\xi] \quad (25)$$

$$\lambda_s=\sqrt{\frac{1}{\kappa_z}(\omega^2+\kappa_y\xi^2)} \quad (26)$$

$$\lambda_0 = \beta_0^2\kappa_z - \kappa_y\xi^2 - \omega^2 \tag{27}$$

$$\lambda_n = \beta_n^2\kappa_z + \kappa_y\xi^2 + \omega^2 \tag{28}$$

where ω and ξ are the variables of $\Re$-transform and Fourier transform, respectively; β_0 and β_n are respectively the roots of the following equations:

$$e^{2\beta_0} = \frac{\beta_0\kappa_z - \gamma(\beta_0^2\kappa_z - \kappa_y\xi^2 - \omega^2)}{\beta_0\kappa_z + \gamma(\beta_0^2\kappa_z - \kappa_y\xi^2 - \omega^2)} \tag{29}$$

$$\tan(\beta_n) = -\frac{\gamma(\beta_n^2\kappa_z + \kappa_y\xi^2 + \omega^2)}{\beta_n\kappa_z} \tag{30}$$

Note that Eq. (30) has infinite roots because of the function $\tan(\beta_n)$, and the positive roots of Eqs. (29) and (30) are chosen for evaluating the integration of Eqs. (16) and (17). The roots of Eqs. (29) and (30) are close to the location of vertical asymptotes. The asymptote for Eq. (29) can be derived from letting its denominators be zero. The asymptote for Eq. (30) results from the function $\tan(\beta_n)$. Therefore, the roots of Eqs. (29) and (30) can be obtained by Newton's method with the initial guesses $[-\kappa_z + \sqrt{\kappa_z^2 + 4\kappa_z\gamma^2(\kappa_y\xi^2 + \omega^2)}]/(2\kappa_z\gamma) + 10^{-9}$ and $(2n-1)\pi/2 + 10^{-9}$, respectively, where n is an integer from $1, 2, 3, \ldots, \infty$ and 10^{-9} represents a small shift to avoid initial guesses being located at the vertical asymptotes.

The solution for describing head distributions induced by a radial collector well with several laterals is obtained by dividing the sum of all lateral length and by integrating the point-sink solution, Eqs. (16) and (17), along all laterals. Such integration is based on the assumption that the discharge intensity, defined as $Q/(L_i + \cdots + L_N)$, is a constant over all of laterals. The result is expressed as

$$h_{aR}(x_D, y_D, z_D, t_D) = \sum_{i=1}^{N} \frac{1}{L_{Di} + \cdots + L_{DN}} \int_0^{L_{Di}} h_{Da}\,dl \quad \text{for} \quad z_{0D} \leqslant z_D \leqslant 0 \tag{31}$$

$$h_{bR}(x_D, y_D, z_D, t_D) = \sum_{i=1}^{N} \frac{1}{L_{Di} + \cdots + L_{DN}} \int_0^{L_{Di}} h_{Db}\,dl \quad \text{for} \quad -1 \leqslant z_D \leqslant z_{0D} \tag{32}$$

with

$$x'_D = l\cos(\theta_i) + x_{0D} \tag{33}$$

$$y'_D = l\sin(\theta_i) + y_{0D} \tag{34}$$

$$z'_D = z_{0D} \tag{35}$$

where l is a dummy variable, N is the number of the laterals, and subscript i represents the ith lateral. The steady-state head solutions for Eqs. (31) and (32) can be obtained by neglecting Φ_0, Φ_n, Ψ_0, and Ψ_n where the exponential terms become small when time goes very large.

2.3. Stream depletion rate

Based on Darcy's law, filtration from a stream can be written as

$$q = -\int_\Omega K'\frac{h}{b'}\,dA \quad at \quad x_D = 0 \tag{36}$$

where Ω represents the whole domain of the streambed and h represents dimensional hydraulic head for the aquifer at $x_D = 0$. According to dimensionless variables and Eqs. (31) and (32), the SDR can be written as

$$SDR = \frac{q}{Q} = \frac{\alpha}{\pi^2}\int_{-\infty}^{\infty}\left(\int_{z_{0D}}^{0} h_{aR}\,dz_D + \int_{-1}^{z_{0D}} h_{bR}\,dz_D\right)dy_D \quad at \quad x_D = 0 \tag{37}$$

2.4. Numerical evaluations

The integrals of Eqs. 31, 32, and 37 can be calculated by using Gaussian quadrature (e.g., Gerald and Wheatley, 2004). The integrands in these three equations exhibit oscillatory behaviors because of trigonometric functions. Each of these integrals can be expressed as a sum of infinite series and each term of the series can be determined by calculating the area between two consecutive roots of the integrand along ξ or ω axis. In addition, each area is evaluated by 3-term Gaussian quadrature formula. The series converges quickly and generally takes about 20 terms to achieve an accuracy of centimeter.

3. Results and discussion

Table 1 shows the default dimensional parameters for the studies in following sections. The aquifer is of anisotropy with vertical hydraulic conductivity smaller than horizontal one. A radial collector well is considered to have three laterals with equal length, and the configuration of the lateral is symmetric to center of the well as demonstrated in Fig. 2 for the top view.

3.1. Comparison with Hantush and Papadopoulos' long-time solution (1962)

Hantush and Papadopoulos (1962) presented short-time and long-time solutions describing drawdown distributions induced by pumping at a radial collector well in an isotropic unconfined aquifer extending infinitely. In other words, their solutions can give good accuracy in predicting head only using the short-time solution for small pumping time and the long-time solution for large pumping time.

The present solution can be used to predict head over the whole time domain and can simulate head distributions in an aquifer extending infinitely. The well is located at x = 150 m which is far away from the stream, and the drawdown cone does not reach the stream. Fig. 2 shows spatial head distributions at the elevation of installing the well predicted by their large-time solution and the present solution. The radius of the caisson is considered as 0.1 m in their solution for the comparison with the present solution. The aquifer is isotropic with the conductivities $K_x = K_y = K_z$ = 1 m/day. The time is set as 210 days for their large-time solution. The thick

Table 1
The default values of dimensional parameters.

Parameter	Value
K_x (m/day)	1
K_y (m/day)	1
K_z (m/day)	0.1
K' (m/day)	0.1
b' (m)	1
S_s (1/m)	10^{-4}
S_y	0.3
H (m)	10
N (lateral number)	3
$L_1 = L_2 = L_3$ (m)	10
Q (m^3/day)	10
x_0 (m)	20
y_0 (m)	0
z_0 (m)	−8
θ_1	0
θ_2	$2\pi/3$
θ_3	$4\pi/3$

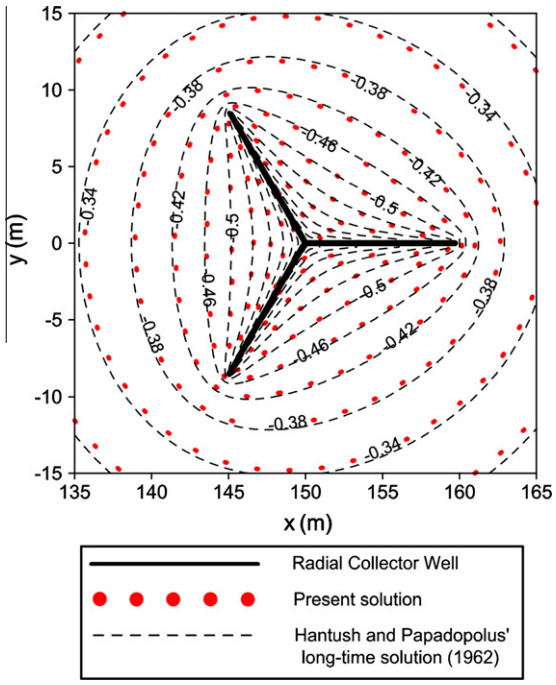

Fig. 2. Spatial head distributions predicted from Hantush and Papadopulos' long-time solution (1962) and the present solution at $z = z_0$ when $t = 210$ days.

solid lines represent the laterals of the collector well. The contours of head predicted from the present solution are denoted by the dotted lines, and those from their solution are represented by the dashed lines. The figure shows that, the contours of the predicted heads from both solutions match very well, especially near the laterals. These results indicate that the present solution has a good performance in simulating head distributions in an aquifer of infinite extent.

3.2. Comparison with Hantush's solution (1965)

Hantush (1965) presented an analytical solution for describing head distributions induced by pumping at a fully-penetrating vertical well in an aquifer near a stream. The vertical flow is neglected based on the Dupuit assumption. The aquifer is of semi-infinite extent in the horizontal direction. The stream fully penetrating the aquifer is treated as a third-type boundary.

The steady-state water table predicted from Hantush's solution (1965) for pumping at a vertical well and from the present solution for a radial collector well with three laterals are compared for $y = 0$ and 200 m as shown in Fig. 3. For the case of $y = 0$, the head from the present solution is larger than that from Hantush's solution (1965) between $x = 0$ m and $x = 50$ m. The collector well produces significantly smaller drawdown than the vertical well as shown in the figure. This is because the collector well has three laterals extending with $L_1 = L_2 = L_3 = 10$ m. The area where groundwater is pumped by the collector well distributes much wider than that of the vertical well. The difference between the present solution and Hantush's solution (1965) is however very small in the case of $y = 200$ m for $-\infty \leqslant x \leqslant \infty$ and in the case of $y = 0$ for $x \geqslant 100$ m. This reflects that the effect of well type on the head distributions is insignificant for those locations far away from the well.

3.3. Effect of streambed on SDR and head

Steady-state SDR depends only on the ratio of streambed permeability K' over aquifer permeability K_x. Substituting the first terms of Eqs. (31) and (32) into Eq. (37) yields steady-state SDR which is independent of time. The type curve of steady-state SDR versus the ratio of K'/K_x is shown in Fig. 4. When $K'/K_x \geqslant 10^{-2}$, the value of the steady-state SDR is one, indicating that the filtration rate from a stream to an aquifer is equal to the discharge extracted from a well. The large drawdown therefore happens in a small area in the range of $0 \leqslant x \leqslant 200$ m as shown in Fig. 5 for the cases of $K'/K_x \geqslant 10^{-2}$. Note that no discontinuity in water table between the aquifer and stream happens as shown in Fig. 5 for the case of $K'/K_x = 1$, and the streambed can be regarded as a part of the aquifer. Under such a condition, Eq. (2) can be replaced by a constant-head boundary, $h = 0$. When $K'/K_x < 10^{-2}$, the value of the steady-state SDR is less than one. The filtration rate is less than the well extraction rate. Such a problem produces deep and wide drawdown cones as shown in Fig. 5 for $K'/K_x < 10^{-2}$. When $K'/K_x < 10^{-7}$, the value of the steady-state SDR is zero. The filtration does not happen for the entire period of pumping time, and the

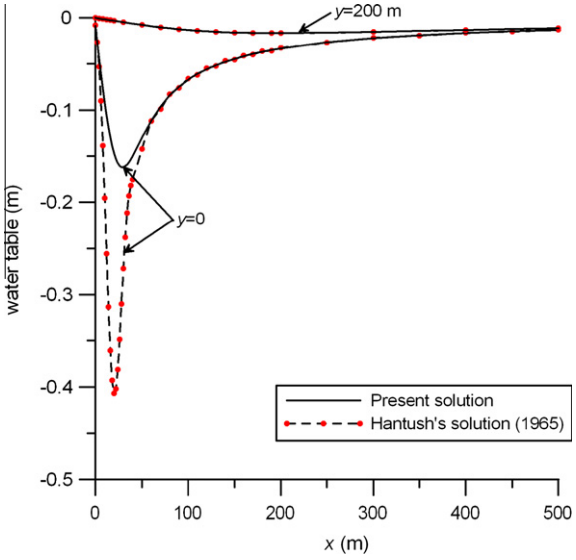

Fig. 3. Steady-state head distributions at water table predicted from Hantush's solution (1965) and the present solution at $z = 0$ for various y.

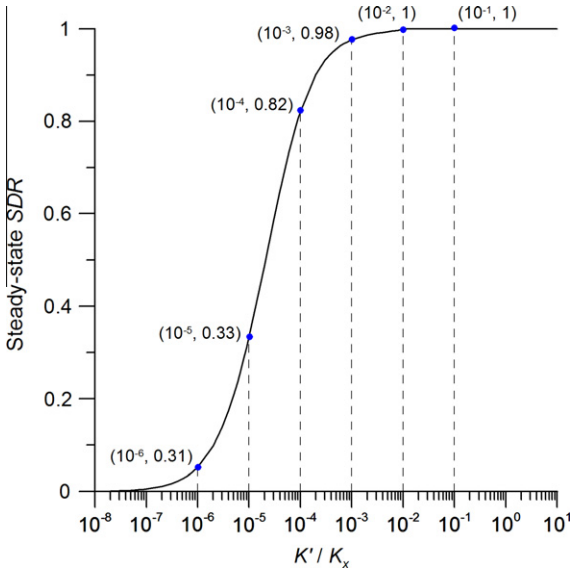

Fig. 4. Type curve of steady-state SDR versus K'/K_x.

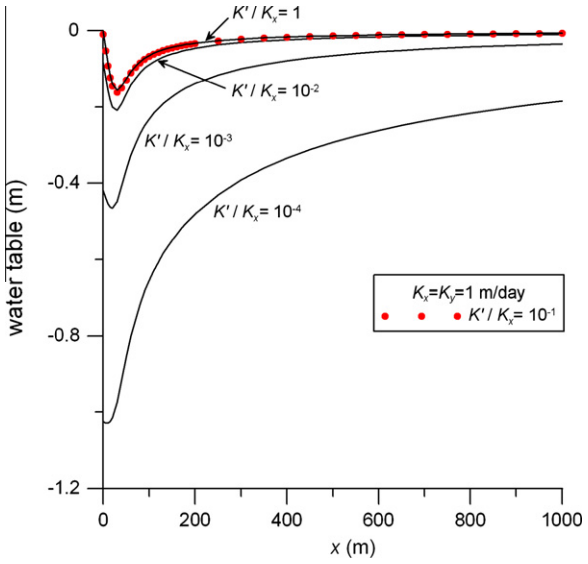

Fig. 5. Steady-state head distributions at water table due to pumping in a radial collector well with three symmetrical laterals at $y = 0$ for various K'/K_x.

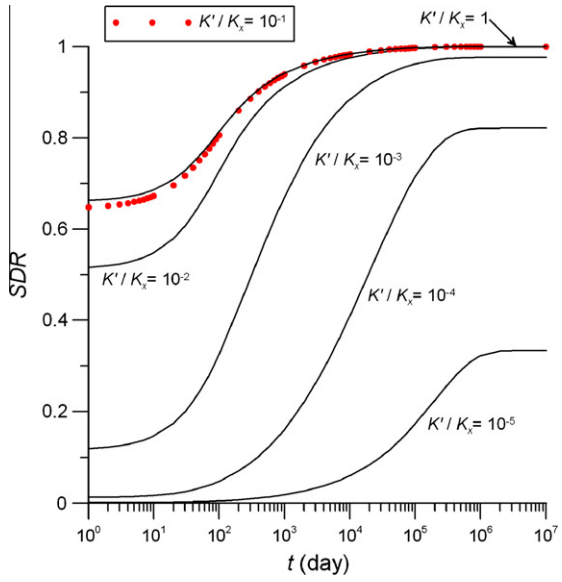

Fig. 6. Temporal distribution curves of SDR for various K'/K_x.

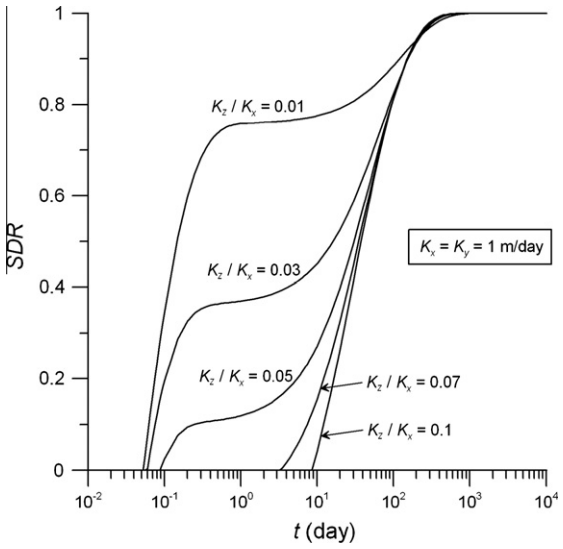

Fig. 7. Temporal distribution curves of SDR due to pumping in a radial collector well with three symmetrical laterals for various K_z/K_x.

streambed is indeed a no-flow boundary. Under such a circumstance, Eq. (2) can be replaced by $\partial h/\partial x = 0$.

The permeability of the streambed affects the value of SDR. Fig. 6 shows the curves of temporal SDR for various K'/K_x based on $K_x = 1$ m/day. The curve with a smaller K'/K_x has a smaller value of SDR than those with a larger one. The low permeability of a streambed therefore results in a small filtration rate at a fixed time. For each of curves, the SDR increases with time and then reaches steady state at different values as expected in Fig. 4. It is worth noting that the difference between the curves with $K'/K_x = 1$ and $K'/K_x = 10^{-1}$ is very small. This is because the permeability of the streambed is close to that of the aquifer.

3.4. Effect of vertical hydraulic conductivity on SDR

The vertical hydraulic conductivity of an aquifer is generally smaller than the horizontal one. The temporal distribution curves of SDR for various K_z are shown in Fig. 7 which exhibits two different patterns of the curves. One has five stages for the cases of $K_z \leqslant 0.05$; this has a period of zero SDR at beginning, a rapid increase at early time, a flat period at middle time, a marked increase again at late time, and an equilibrium state finally. During the first stage, water extracted by a well comes entirely from elastic release due to the compression of the aquifer and the expansion of water. The hydraulic gradient at the stream boundary maintains zero, and thus the SDR is zero. In the second stage, the elastic release slows or stops, and a drawdown cone reaches the stream boundary. The SDR therefore increases with time. During the third stage, gravity drainage from a decline of water table starts to supply the well extraction. The SDR curve therefore becomes flat. During the fourth stage, the gravity drainage diminishes and the SDR increases again. Finally, the groundwater flow reaches steady state and all the water extracted from the well is from the stream in the equilibrium state. For the cases of $K_z > 0.05$, there are three stages as shown in Fig. 7 including a period of zero SDR at early time, a conjunctive water supply from the stream to the aquifer in the intermediate period, and finally the equilibrium state. In addition, Fig. 7 also shows that the aquifer with a smaller K_z has larger SDR than that with a larger one, indicating that a smaller K_z results in less water from the gravity drainage and more water from the stream for a fixed pumping rate.

3.5. Location of lowest water table

The location of the lowest water table depends on the period of filtration from a stream to an aquifer. Fig. 8 displays the contours of temporal water table distributions for pumping times at 0.001, 0.01, 1, and 100 days. The contours distribute over $10 \leqslant x \leqslant 30$ and $-10 \leqslant y \leqslant 10$ at $t = 0.001$ day shown in Fig. 8a, indicating that the drawdown cone has not yet touched the stream, and thus filtration has not started. The lowest water table appears exactly at the center of the well (i.e., $x = 20$ m and $y = 0$), and the contours reflects the lateral configuration. The drawdown cone has touched the stream at $t = 0.01$ day indicated in Fig. 8b and the lowest head is still near the center of the well. As the time elapses, the filtration from the stream recharges the adjacent aquifer and consequently the lowest head moves away from the stream. The profile of the contours moves landward and turns into a circle as displayed in Fig. 8c at $t = 1$ day and in Fig. 8d at $t = 100$ day.

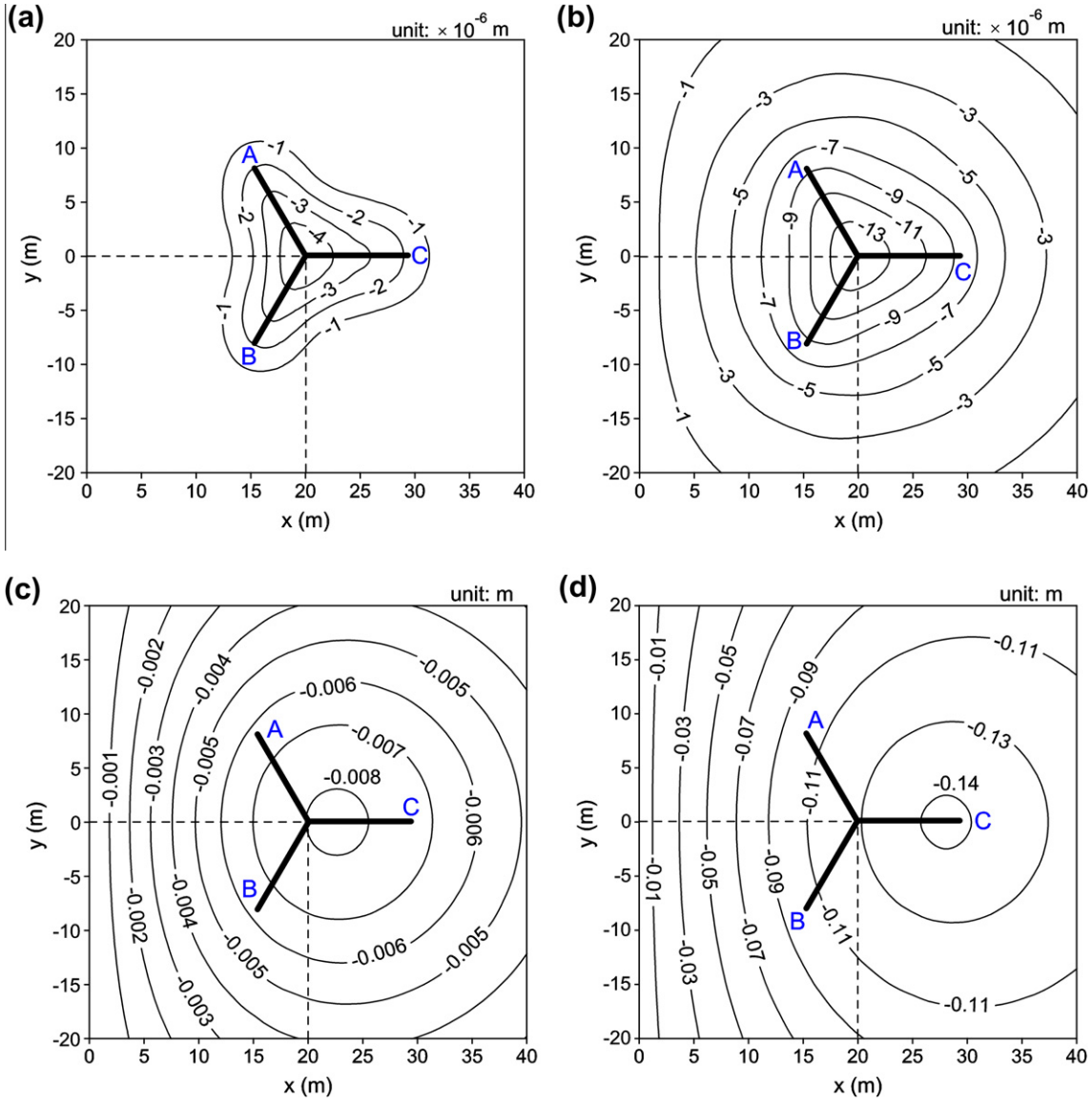

Fig. 8. The contours of transient water table due to pumping in a radial collector well with three symmetrical laterals for various times. (a) $t = 0.001$ day. (b) $t = 0.01$ day. (c) $t = 1$ day. (d) $t = 100$ day.

Those figures indicate that the water pumped by the laterals A and B comes mainly from filtration for the aquifer near the stream (i.e., $0 \leqslant x \leqslant 20$) and the drawdown in this area is therefore small. On the other hand, the water pumped by the lateral C comes mainly from groundwater in the inland area for $x \geqslant 20$ and the drawdown in this region is therefore large.

3.6. Effect of different lateral configuration on water table and SDR

Fig. 9 shows the contours of water table due to pumping from a radial collector well in four cases with different lateral configurations. Case (a) is designed for the scenario with symmetrical laterals to the center of the well, case (b) for non-symmetrical laterals, case (c) for the laterals toward a stream, and case (d) for the laterals landward. Among these four cases, case (c) has the least drawdown contour because its laterals are closer to the stream and obtain more water from the stream. Therefore, the highest SDR in case (c) can be expected as demonstrated in Fig. 10. On the other hand, case (d) has the lowest SDR because its laterals are landward. In addition, case (b) has a smaller drawdown contour and larger SDR in comparison with case (a) because the laterals A and B in case (b) are slightly closer to the stream than those in case (a) as shown in Fig. 9.

The number of symmetrical laterals has insignificant effects on SDR. Fig. 11 illustrates temporal SDR for collector wells with different number N of a symmetrical lateral configuration. There is no difference between those three curves of $L = 10$ m since the shortest distance between the stream and well is almost the same. The curve of $L = 20$ m however has a slightly larger SDR than those of $L = 10$ m when the number of lateral is the same, i.e., $N = 5$. This is because the long lateral has a shorter distance to the stream and results in more water from the stream.

3.7. Comparison with field data from Schafer (2006)

Schafer (2006) carried out a constant-rate pumping test for a collector well with seven laterals near Ohio River in Louisville, Kentucky. The data of the well configuration is listed in Table 2 and the data of aquifer parameters is given in Table 3. During the pumping period of 70 days, the pumping rate Q_1 was maintained

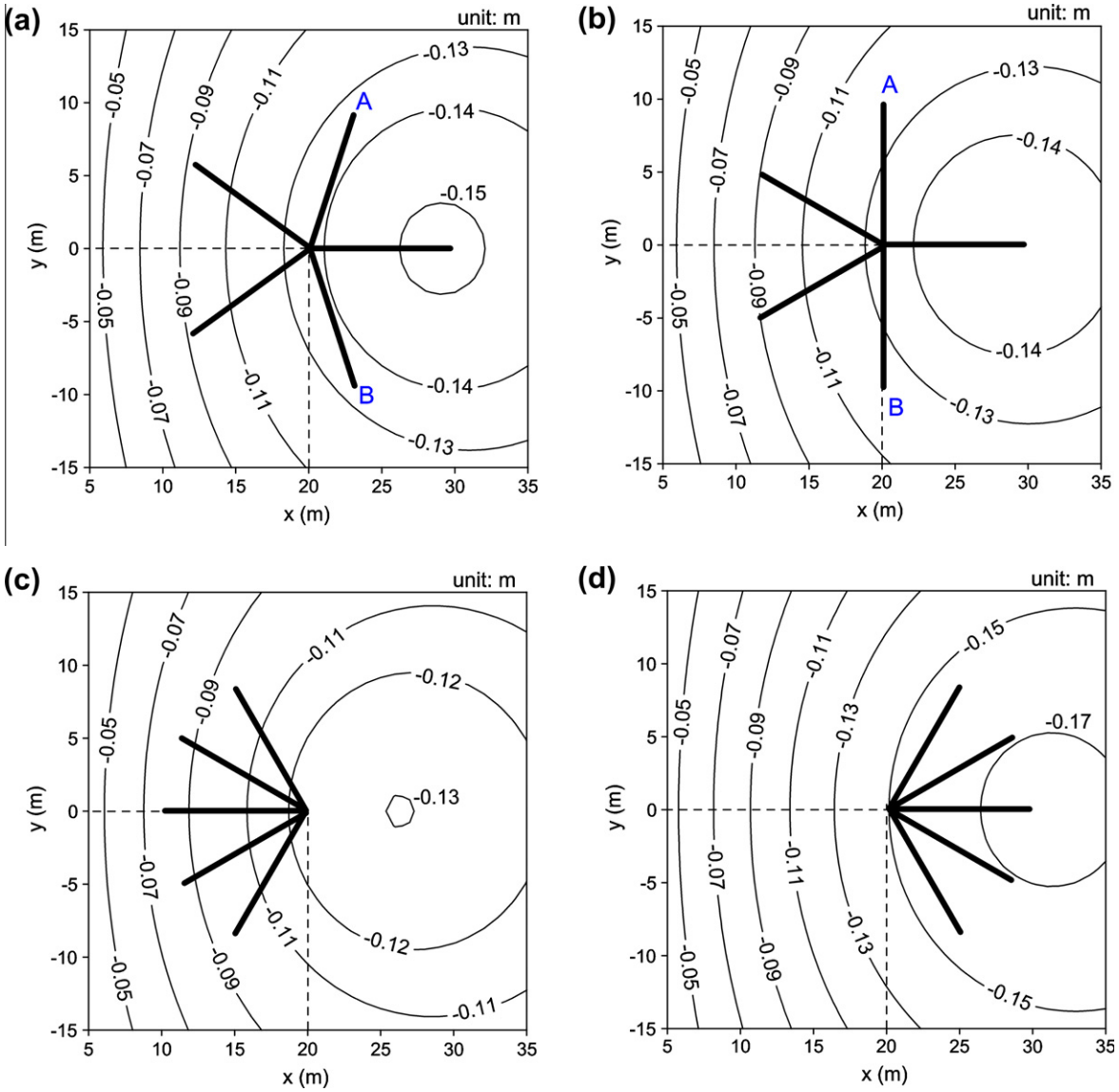

Fig. 9. The contours of steady-state water table due to pumping in a radial collector well with four different configurations. (a) Symmetry, (b) non-symmetry, (c) laterals toward stream, and (d) laterals landward.

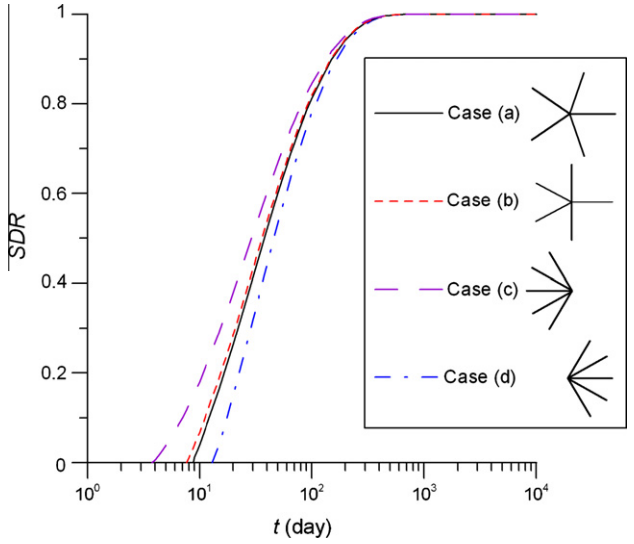

Fig. 10. Temporal distribution curves of SDR for four different lateral configurations.

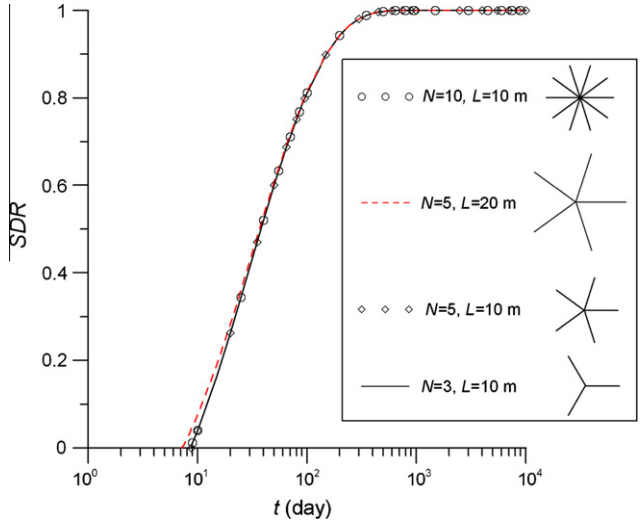

Fig. 11. Temporal distribution curves of SDR for various lateral number and length.

Table 2
The data for the configuration of the radial collector well installed near Ohio River in Louisville, Kentucky.

Lateral data	Value
L_1 (m)	61
L_2 (m)	61
L_3 (m)	61
L_4 (m)	73
L_5 (m)	73
L_6 (m)	73
L_7 (m)	73
θ_1	0
θ_2	$\pi/2$
θ_3	$3\pi/2$
θ_4	$7\pi/10$
θ_5	$9\pi/10$
θ_6	$11\pi/10$
θ_7	$13\pi/10$

Table 3
The parameter values for the aquifer near Ohio River in Louisville, Kentucky.

Parameter	Value
K_x (m/day)	119
K_y (m/day)	119
K_z (m/day)	40
K'/b' (1/day)	2.35
S_s (1/m)	3.64×10^{-5}
S_y	0.3
H (m)	27
x_0 (m)	45
y_0 (m)	0
z_0 (m)	−22.5

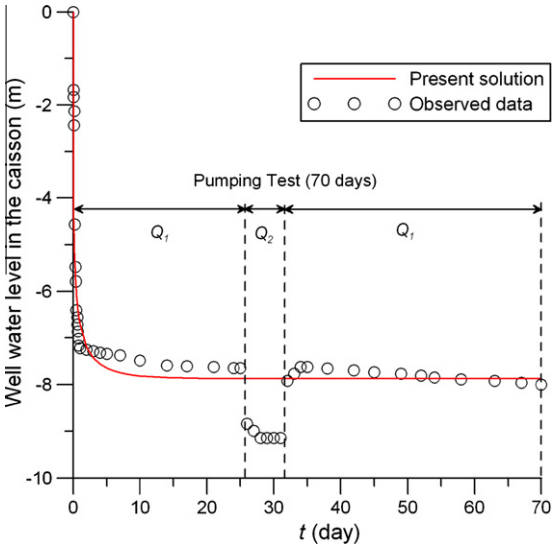

Fig. 12. Water levels predicted by the present solution and the observed field data from Schafer (2006).

about 73,440 m^3/day except in the middle period from 26 to 31 days during which the pumping rate Q_2 was increased to about 81,010 m^3/day as shown in Fig. 12. This figure shows that the water level predicted by the present solution based on the pumping rate 73,440 m^3/day has a good agreement with the water level observed in the caisson over the whole pumping period except in the middle period. The discrepancy reflects the increase of the pumping rate in that period. The slight difference at early pumping period may result from a larger hydraulic conductivity of the aquifer near Ohio River than that away from the river.

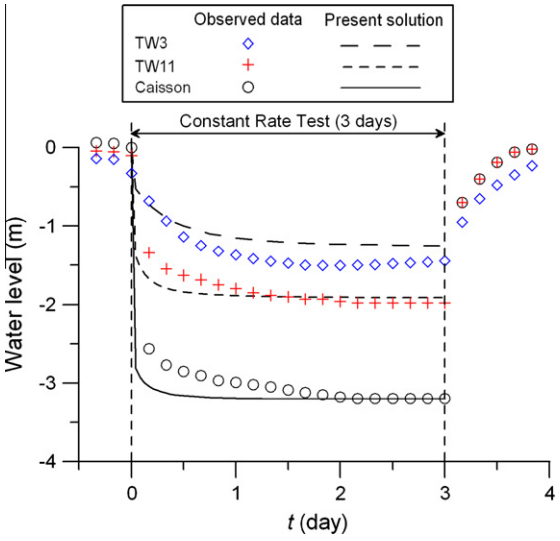

Fig. 13. Water levels predicted by the present solution and the observed field data from Jasperse (2009).

Table 4
The data for the configuration of the radial collector well near Russian River in California.

Lateral data	Value
L_1 (m)	21.3
L_2 (m)	48.8
L_3 (m)	51.8
L_4 (m)	30.5
L_5 (m)	27.4
L_6 (m)	24.4
L_7 (m)	39.6
L_8 (m)	33.5
L_9 (m)	48.8
L_{10} (m)	42.7
θ_1	$5\pi/36$
θ_2	$5\pi/18$
θ_3	$11\pi/18$
θ_4	$38\pi/45$
θ_5	$41\pi/36$
θ_6	$23\pi/18$
θ_7	$3\pi/2$
θ_8	$29\pi/18$
θ_9	$83\pi/45$
θ_{10}	$35\pi/18$

Table 5
The parameter values for the aquifer near Russian River in California.

Parameter	Value
K_x (m/day)	650
K_y (m/day)	650
K_z (m/day)	216.7
K'/b' (1/day)	0.2
S_s (1/m)	4×10^{-5}
S_y	0.3
H (m)	25
x_0 (m)	107
y_0 (m)	0
z_0 (m)	−16.8
(x, y) of TW3	(224.2, −40.3)
(x, y) of TW11	(119, −16.5)

3.8. Comparison with field data from Jasperse (2009)

Jasperse (2009) also executed a constant-rate pumping test for a collector well with 10 laterals near Russian River in California.

Fig. 13 reveals the water level predicted by the present solution with a pumping rate of 67,390 m^3/day and the observed water level measured from the caisson and two monitoring wells: TW3 and TW11. The data of the well configuration are given in Table 4 and the values of aquifer parameters are listed in Table 5. The distances measured from the caisson to TW3 and TW11 are 124 and 20 m, respectively. The well water level predicted by the present solution fairly agrees with the observed water level for the cases of Caisson and TW11. However, the predicted water level by the present solution slightly differs from the observed one for the case of TW3. Such a difference may be caused by aquifer heterogeneity since the distance between the caisson and TW3 is large.

4. Concluding remarks

An analytical solution is developed for describing transient hydraulic head for pumping from a radial collector well in an unconfined aquifer near a stream. The aquifer is considered to be homogenous and anisotropic. The streambed connecting the stream and aquifer is treated as a third-type boundary. The first-order free surface equation is used to describe the hydraulic head at water table. The head solution is derived by $\Re$-transform, Fourier transform and Laplace transform. The temporal SDR is derived according to Darcy's law and the head solution. The steady-state head or SDR solution can be obtained by neglecting the exponential terms involved in time. The present solution gives very good predicted head distributions when compared with those from Hantush and Papadopoulos' long-time solution (1962) under the condition that the collector well is installed far away from the steam. According to the comparison of head distributions from the present solution with those from Hantush's solution (1965), a collector well results in smaller drawdown than a vertical well if adopting several long laterals. The solution is also used to predict hydraulic head near the caisson of the collector well for the real-world cases given in Schafer (2006) and Jasperse (2009). The predicted results seem to be reasonable when compared with observed field data. Some behaviors of groundwater flow caused by pumping in a collector well are investigated and the conclusions can be made below:

1. The steady-state SDR depends only on the ratio of K'/K_x. If $K'/K_x \geqslant 10^{-2}$, steady-state SDR is one. If $K'/K_x < 10^{-7}$, steady-state SDR is zero. If $10^{-7} < K'/K_x \leqslant 10^{-2}$, steady-state SDR increases from 0 to 1 with K'/K_x.
2. If $K'/K_x \leqslant 10^{-2}$, a deep and wide drawdown cone is eventually produced for a long period of pumping time.
3. A streambed with a lower permeability than an aquifer results in a smaller SDR for a fixed time.
4. The curve of temporal SDR for an unconfined aquifer has a middle flat period due to gravity drainage from water table. However, this flat period vanishes gradually with increasing K_z.
5. Before the occurrence of filtration, the largest drawdown occurs right at the center of a collector well. Once the filtration starts to recharge the aquifer, the largest drawdown begins to move landward and away from the center of a collector well.
6. The collector well obtains more SDR and produces less drawdown if the laterals are installed toward the stream.
7. The effect of the lateral number on SDR is insignificant if the laterals are symmetric to the center of a collector well.

Acknowledgements

This study was supported by Taiwan National Science Council under the Grants NSC 99-2221-E-009-062-MY3, NSC 100-2221-E-009-106, and NSC 101-3113-E-007-008. The authors would like to appreciate three anonymous reviewers for their insightful and constructive comments.

Appendix A. Derivation of Eqs. (16) and (17)

A general transform called $\Re$-transform (Sneddon, 1972, pp. 70–76; Sun and Zhan, 2007), combining Fourier sine and Fourier cosine transforms, is applied to Eq. (9) along with the third-type boundary condition, Eq. (10). The transform is defined by following relations

$$F(\omega) = \Re\{f(x)\} = \sqrt{\frac{2}{\pi}}\int_0^\infty f(x)\frac{\omega\cos(\omega x) - \alpha\sin(\omega x)}{\sqrt{\omega^2+\alpha^2}}dx \tag{A.1}$$

$$f(x) = \Re^{-1}\{F(\omega)\} = \sqrt{\frac{2}{\pi}}\int_0^\infty F(\omega)\frac{\omega\cos(\omega x) - \alpha\sin(\omega x)}{\sqrt{\omega^2+\alpha^2}}d\omega \tag{A.2}$$

and has a property that

$$\Re\left\{\frac{\partial^2 f}{\partial x^2}\right\} = -\omega^2 F(\omega) - \sqrt{\frac{2}{\pi}}\omega\left[\frac{\partial f}{\partial x} + \alpha f\right] \tag{A.3}$$

where ω is the variable of $\Re$-transform and α is a constant arisen from the third-type boundary condition. Note that a necessary requirement for satisfying Eq. (A.3) is $\lim_{x\to\infty} f(x) = 0$. Applying $\Re$-transform, Fourier transform and Laplace transform sequentially to Eqs. (9)–(15) to remove the variables of x_D, y_D and t_D results in an ordinary differential equation (ODE) and boundary conditions in terms of z_D as

$$\kappa_z\frac{\partial^2\bar{h}_D}{\partial z_D^2} - (p+\omega^2+\kappa_y\xi^2)\bar{h}_D = \frac{A}{p}\delta(z_D - z'_D) \tag{A.4}$$

$$\kappa_z\frac{\partial\bar{h}_D}{\partial z_D} = -\gamma p\bar{h}_D \quad at \quad z_D = 0 \tag{A.5}$$

$$\frac{\partial\bar{h}_D}{\partial z_D} = 0 \quad at \quad z_D = -1 \tag{A.6}$$

with

$$A = \pi e^{i\xi y'_D}\frac{\omega\cos(\omega x'_D) - \alpha\sin(\omega x'_D)}{\sqrt{\omega^2+\alpha^2}} \tag{A.7}$$

where i is an imaginary unit; ω and ξ are the variables of $\Re$-transform and Fourier transform, respectively.

Due to the property of Dirac delta function, Eq. (A.4) turns into two homogeneous equations as

$$\kappa_z\frac{\partial^2\bar{h}_{Da}}{\partial z_D^2} - (p+\omega^2+\kappa_y\xi^2)\bar{h}_{Da} = 0 \quad for \quad z'_D \leqslant z_D \leqslant 0 \tag{A.8}$$

$$\kappa_z\frac{\partial^2\bar{h}_{Db}}{\partial z_D^2} - (p+\omega^2+\kappa_y\xi^2)\bar{h}_{Db} = 0 \quad for \quad -1 \leqslant z_D \leqslant z'_D \tag{A.9}$$

where $\bar{h}_{Da}$ and $\bar{h}_{Db}$ represent hydraulic head in Laplace and Fourier domains above and below z'_D, respectively. The hydraulic head is continuous at $z = z'_D$; therefore, a continuity requirement at $z_D = z'_D$ can be expressed as

$$\bar{h}_{Da} = \bar{h}_{Db} \quad at \quad z_D = z'_D \tag{A.10}$$

In contrast, the hydraulic gradient is discontinuous at $z_D = z'_D$ due to Dirac delta function. Integrating Eq. (A.4) from $z_D = z'^-_D$ to $z_D = z'^+_D$ yields another continuity requirement at $z_D = z'_D$ as

$$\frac{\partial \bar{h}_{Da}}{\partial z_D} - \frac{\partial \bar{h}_{Db}}{\partial z_D} = \frac{A}{\kappa_z p} \quad at \quad z_D = z'_D \tag{A.11}$$

Solve Eqs. (A.8) and (A.9) simultaneously with boundary conditions, Eqs. (A.5), (A.6), and continuity requirements, Eqs. (A.10) and (A.11). One can obtain the solution in Fourier and Laplace domains as

$$\bar{h}_{Da} = \frac{A\cosh[(1+z'_D)\lambda][-\kappa_z\lambda\cosh(z_D\lambda) + p\gamma\sinh(z_D\lambda)]}{p\kappa_z\lambda[\kappa_z\lambda\sinh(\lambda) + p\gamma\cosh(\lambda)]} \quad \text{for} \quad z'_D \leqslant z_D \leqslant 0 \tag{A.12}$$

$$\bar{h}_{Db} = \frac{A\cosh[(1+z_D)\lambda][-\kappa_z\lambda\cosh(z'_D\lambda) + p\gamma\sinh(z'_D\lambda)]}{p\kappa_z\lambda[\kappa_z\lambda\sinh(\lambda) + p\gamma\cosh(\lambda)]} \quad \text{for} \quad -1 \leqslant z_D \leqslant z'_D \tag{A.13}$$

where

$$\lambda = \sqrt{\frac{(p + \omega^2 + \kappa_y\xi^2)}{\kappa_z}} \tag{A.14}$$

Multiplying the term of $e^{p t_D}$ to the right-hand sides of Eqs. (A.12) and (A.13) because of the definition of inverse Laplace transform results in two single-value functions to the variable p. Accordingly, the inverse Laplace transform to Eqs. (A.12) and (A.13) can be obtained by summing the residues of poles in complex plane based on Bromwich integral (Yeh and Yang, 2006).

The poles are the roots of equations derived by letting the denominator of Eqs. (A.12) and (A.13) to be zero. Note that the denominator of Eq. (A.12) is the same as that of Eq. (A.13). One pole obviously occurs at $p = 0$ while the other poles at negative position of the real axis in which one pole p_0 exists between $p = 0$ and $p = -(\omega^2 + \kappa_y\xi^2)$ and infinite poles p_n happen behind $p = -(\omega^2 + \kappa_y\xi^2)$. For the expression without i, substituting $p = p_0$ into Eq. (A.14) and then letting $\lambda = \beta_0$ lead to $p_0 = \kappa_z\beta_0^2 - \omega^2 - \kappa_y\xi^2$. Note that β_0 is a positive value because p_0 is located between $p = 0$ and $p = -(\omega^2 + \kappa_y\xi^2)$. Similarly, substituting $p = p_n$ into Eq. (A.14) and then letting $\lambda = i\beta_n$ result in $p_n = -\kappa_z\beta_n^2 - \omega^2 - \kappa_y\xi^2$ where β_n is also positive values since p_n is smaller than $-(\omega^2 + \kappa_y\xi^2)$. Eventually, substituting $p = p_0$ and $p_0 = \kappa_z\beta_0^2 - \omega^2 - \kappa_y\xi^2$ into the denominator of Eq. (A.12) and then letting the result to be zero yield Eq. (29). In a similar matter, substituting $p = p_n$ and $p_n = -\kappa_z\beta_n^2 - \omega^2 - \kappa_y\xi^2$ into the same denominator and then letting the result to be zero yield Eq. (30).

With known locations of the poles in the complex plane, the residues of the poles for Eqs. (A.12) and (A.13) can be estimated by

$$\mathrm{Res}|_{p=p_N} = \lim_{p\to p_N} f(p)e^{pt_D}(p - p_N) \tag{A.15}$$

where $\mathrm{Res}|_{p=p_N}$ represents the residue of the pole p_N for $f(p)$, and $f(p)$ represents $\bar{h}_{D\,a}$ in Eq. (A.12) or $\bar{h}_{D\,b}$ in Eq. (A.13). The residues for Eq. (A.12) are first estimated and thus $f(p) = \bar{h}_{D\,a}$. The residue at $p = 0$ can be determined by substituting $p_N = 0$ into Eq. (A.15). The result is

$$\mathrm{Res}|_{p=0} = -\frac{A\cosh[(1+z'_D)\lambda]\cosh(z_D\lambda)}{\kappa_z\lambda\sinh(\lambda)} \tag{A.16}$$

Substituting $\lambda = \beta_0$ and $p_N = p_0 = \kappa_z\beta_0^2 - \omega^2 - \kappa_y\xi^2$ into Eq. (A.15) and then applying L'Hopital's rule result in the residue at $p = p_0$ as

$$\mathrm{Res}|_{p=p_0} = -\frac{2A\cosh[(1+z'_D)\beta_0](\beta_0\kappa_z\cosh(z_D\beta_0) - \gamma\lambda_0\sinh(z_D\beta_0))}{\lambda_0[(1+2\gamma)\beta_0\kappa_z\cosh(\beta_0) + (\kappa_z + \gamma\lambda_0)\sinh(\beta_0)]}e^{\lambda_0 t_D} \tag{A.17}$$

Similarly, the residue at $p = p_n$ can be obtained by substituting $\lambda = i\beta_n$ and $p_N = p_n = -\kappa_z\beta_n^2 - \omega^2 - \kappa_y\xi^2$ into Eq. (A.15) and applying L'Hopital's rule as

$$\mathrm{Res}|_{p=p_n} = \frac{2A\cos[(1+z'_D)\beta_n](\beta_n\kappa_z\cos(z_D\beta_n) + \gamma\lambda_n\sin(z_D\beta_n))}{\lambda_n[(1+2\gamma)\beta_n\kappa_z\cos(\beta_n) - (\kappa_z + \gamma\lambda_n)\sin(\beta_n)]}e^{-\lambda_n t_D} \tag{A.18}$$

The sum of Eqs. (A.16)–(A.18) is the inverse Laplace transform of Eq. (A.12). Eventually, taking the inverse Fourier transform and $\Re$-transform yields head solution, Eq. (16). Similarly, based on the derivation of Eq. (16) shown above, Eq. (17) can also be obtained from Eqs. (A.13) and (A.15) in a similar manner.

References

Bakker, M., Kelson, V.A., Luther, K.H., 2005. Multilayer analytic element modeling of radial collector wells. Ground Water 43 (6), 926–934. http://dx.doi.org/10.1111/j.1745-6584.2005.00116.

Bischoff, H., 1981. An integral equation method to solve three dimensional confined flow to drainage systems. Appl. Math. Model. 5 (6), 399–404.

Dugat, W.D., 2009. Interactions and implications of a collector well with a river in an unconfined aquifer with regional background flow. PhD Thesis, Texas A&M University.

Gerald, C.F., Wheatley, P.O., 2004. Applied Numerical Analysis, seventh ed. Addison-Wesley, California.

Hantush, M.S., 1965. Wells near streams with semi-pervious beds. J. Geophys. Res. 70 (12), 2829–2838.

Hantush, M.S., Papadopoulos, I.S., 1962. Flow of groundwater to collector wells. J. Hydr. Eng. Div. – ASCE 88 (5), 221–244.

Huang, C.S., Chen, Y.L., Yeh, H.D., 2011. A general analytical solution for flow to a single horizontal well by Fourier and Laplace transforms. Adv. Water Resour. 34 (5), 640–648. http://dx.doi.org/10.1016/j.advwatres.2011.02.015.

Hunt, H., 2006. American experience in installing horizontal collector wells. Water Sci. Technol. Libr. 43 (1), 29–34. http://dx.doi.org/10.1007/0-306-48154-5_3.

Intaraprasong, T., Zhan, H., 2009. A general framework of stream-aquifer interaction caused by variable stream stages. J. Hydrol. 373 (1–2), 112–121. http://dx.doi.org/10.1016/j.jhydrol.2009.04.016.

Jacob, C.E., 1950. Engineering Hydraulics. John Wiley & Sons, New York.

Jasperse, J., 2009. Planning, design and operations of collector 6, Sonoma County Water Agency. NATO Science for Peace and Security Series 169–202. http://dx.doi.org/10.1007/978-94-007-0026-0_11.

Javandel, I., Zaghi, N., 1975. Analysis of flow to an extended fully penetrating well. Water Resour. Res. 11 (1), 159–164.

Kim, S.H., Ahn, K.H., Ray, C., 2008. Distribution of discharge intensity along small-diameter collector well laterals in a model riverbed filtration. J. Irrig. Drain. E – ASCE 134 (4), 493–500. http://dx.doi.org/10.1061/(asce)0733-9437(2008)134:4(493).

McWhorter, D.B., Sunada, D.K., 1977. Ground-Water Hydrology and Hydraulics. Water Resources Publications, Englewood, pp. 122–124.

Mikels, F.C., Klaer, F.H., 1956. Application of ground water hydraulics to the development of water supplies by induced infiltration. Int. Assoc. Sci. Hydrol. 41, 232–242.

Mohamed, A., Rushton, K., 2006. Horizontal wells in shallow aquifers: field experiment and numerical model. J. Hydrol. 329, 98–109. http://dx.doi.org/10.1016/j.jhydrol.2006.02.006.

Patel, H.M., Eldho, T.I., Rastogi, A.K., 2010. Simulation of radial collector well in shallow alluvial riverbed aquifer using analytic element method. J. Irrig. Drain. E – ASCE 136 (2), 107–119. http://dx.doi.org/10.1061/(ASCE)IR.1943-4774.0000141.

Schafer, D.C., 2006. Use of aquifer testing and groundwater modeling to evaluate aquifer/river hydraulics at Louisville Water Company, Louisville, Kentucky, USA. NATO Sci. Ser. IV Earth Environ. Sci. 60, 179–198. http://dx.doi.org/10.1007/978-1-4020-3938-6_8.

Sneddon, Ian.N., 1972. The Use of Integral Transforms. McGraw-Hill, New York.

Su, G.W., Jasperse, J., Seymour, D., Constantz, J., Zhou, Q., 2007. Analysis of pumping-induced unsaturated regions beneath a perennial river. Water Resour. Res. 43, W08421. http://dx.doi.org/10.1029/2006WR005389.

Sun, D., Zhan, H., 2006. Flow to a horizontal well in an aquitard-aquifer system. J. Hydrol. 321 (1–4), 364–376. http://dx.doi.org/10.1016/j.jhydrol.2005.08.008.

Sun, D., Zhan, H., 2007. Pumping induced depletion from two streams. Adv. Water Resour. 30 (4), 1016–1026. http://dx.doi.org/10.1016/j.advwatres.2006.09.001.

Todd, D.K., Mays, L.W., 2005. Groundwater Hydrology, third ed. John Wiley & Sons, New York.

Tsou, P.R., Feng, Z.Y., Yeh, H.D., Huang, C.S., 2010. Stream depletion rate with horizontal or slanted wells in confined aquifers near a stream. Hydrol. Earth Syst. Sci. 14 (8), 1477–1485. http://dx.doi.org/10.5194/hessd-7-2347-2010.

Yeh, H.D., Yang, S.Y., 2006. A novel analytical solution for constant-head test in a patchy aquifer. Int. J. Numer. Anal. Met. 30 (12), 1213–1230. http://dx.doi.org/10.1002/nag.523.

Yeh, H.D., Huang, C.S., Chang, Y.C., Jeng, D.S., 2010. An analytical solution for tidal fluctuations in unconfined aquifers with a vertical beach. Water Resour. Res. 46, W10535. http://dx.doi.org/10.1029/2009WR008746.